Liquid crystalline thermosets based on anisotropic phases of cellulose nanocrystals

Justin O. Zoppe,[†] Lucas Grosset,[‡] and Jukka Seppälä[†]*

[†]Polymer Technology, Department of Biotechnology & Chemical Technology, Aalto University School of Chemical Technology, P.O. Box 16100, 00076 Aalto, Finland

[‡]Department of Materials Science & Engineering, INSA Lyon, 7-9 Av. Jean-Capelle, F-69621 Villeurbanne cedex, France

*Corresponding author: E-mail: jukka.seppala@aalto.fi, Phone: +358 40 070 1142, Fax: +358 9 451 2622

KEYWORDS. Cellulose nanocrystals, whiskers, liquid crystalline thermoset, birefringence, epoxy nanocomposite, lyotropic liquid crystals.

ABSTRACT

A new class of liquid crystalline thermosets (LCTs) was successfully produced containing lyotropic cellulose nanocrystals (CNCs) as the primary mesogenic component (up to 72 % wt.) by the addition of non-mesogenic epoxy monomers. Cellulose-based LCTs were produced by totally aqueous processing methods and ultimately cured at elevated temperatures to produce ordered networks of 'frozen' liquid crystalline (LC) phases. Various degrees of birefringence were obtained via self-assembly of cellulose nanocrystals into oriented phases as observed by polarized optical microscopy and transmission electron microscopy. X-ray diffraction measurements highlighted the effects of texture of CNCs within LCT films compared to lyophilized CNCs. Cellulose-based LCT films uniquely exhibited thermo-mechanical properties of both traditional liquid crystalline thermosets and liquid crystalline elastomers, such as high elastic modulus (~1 GPa) under ambient conditions and low glass transition temperature (~ -25 °C), respectively. The development of liquid crystalline thermosets based on cellulose nanocrystals and aqueous processing methods provides a renewable pathway for designing high performance composites with ordered network structures and unique optical properties.

Introduction

"Freezing" liquid crystalline (LC) phases into a highly cross-linked and ordered polymeric network can lead to desirable mechanical and optical properties (Barclay and Ober, 1993; Ortiz et al., 1998a; Shiota and Ober, 1997). Traditionally, this has been accomplished by cross-linking of rigid-rod molecules containing thermotropic mesogens end-capped with functional groups such as acrylates, cyanates, or glycidyl groups. These highly ordered and densely cross-linked network structures prepared by polyaddition/polycondensation processes resulted in a new class of materials termed liquid crystalline thermosets (LCTs). Another related class of materials, called liquid crystalline elastomers (LCEs), provide more loosely cross-linked networks prepared by similar processes (Giamberini et al., 2005; Ortiz et al., 1998b; Ribera et al., 2006). The primary advantage of LCTs is enhanced mechanical properties due to heterogeneities and localized anisotropy of nematic structure within an overall isotropic microstructure (Kannan and Sudhakara, 2011). These heterogeneities are suggested to cause deviations in crack propagation from a straight line leading to increased modulus and fracture toughness. In addition to having microscopic domains of uniform orientation, LCTs and LCEs can also be macroscopically oriented by curing in an electric or magnetic field. As one of the most widely used thermosetting materials, epoxy resins represent an important class of LCTs due to unique chemical characteristics such as curing reactions without byproducts, low shrinkage, and controllable cross-linking (Carfagna et al., 1994, 1997). Epoxy-based LCTs can also display unique optical properties due to their anisotropy, such as birefringence useful for nonlinear optics, filters and photorefractive materials (Amendola et al., 1996; Tan and Fung, 2001). Epoxy resins, in general, have a broad range of applications including adhesives, coatings, and composite materials (May and Tanaka, 1973). Their high stiffness and low density make epoxies ideal matrices in fiber-reinforced composites, especially for wind power (Brondsted et al., 2005) and the aircraft industry (Kannan and Sudhakara, 2011).

Cellulose nanocrystals (CNCs) afford significant improvements in the thermo-mechanical properties of a wide range of polymer matrices by adding only small amounts (Habibi et al., 2010; Moon et al., 2011). Also referred to as cellulose whiskers or nanocrystalline cellulose (NCC), cellulose nanocrystals consist of rod-like nanoparticles with widths ranging 5-70 nm and lengths of 100 nm to several microns depending on the source of biomass, thus provide a high aspect ratio reinforcing phase (Bras et al., 2011). Epoxy nanocomposites have been produced using cellulose nanocrystals as a reinforcing phase, while most researchers have focused on solvent exchange, gel templating or lyophilizing CNCs and re-dispersion in the epoxy hardener (Rusli and Eichhorn, 2008, 2011) or in polar organic solvents such as dimethyl formamide (Khelifa et al., 2012; Tang and Weder, 2010). Nevertheless, Ruiz et al. (Ruiz et al., 2000; Ruiz et al., 2001) demonstrated the reinforcing effect of up to 5 % wt. cellulose nanocrystals within a thermoset matrix via a water-based epoxy emulsion system, which avoided solvent-exchange and lyophilization. Given the abundance and biodegradability of cellulose, and the desire to decrease our dependence on petroleum-based chemicals, it would be beneficial to develop high performance composites, which contain cellulose as the major component, *i.e.* the polymer matrix. Some examples of epoxy-based nanocomposites containing high cellulose content have been developed in the form of highly transparent and thermally conductive films using bacterial cellulose (Retegi et al., 2012) and nanofibrillated cellulose (Shimazaki et al., 2007), respectively. However, to the best of our knowledge, the use of cellulose nanocrystals (CNCs) as the major component of liquid crystalline epoxy thermosets has been unexplored.

In addition to the high stiffness and thermal stability of cellulose nanocrystals, negative surface charges derived from sulfuric acid hydrolysis promote uniform dispersions stabilized via electrostatic repulsions (Habibi et al., 2010). This phenomenon leads to their self-assembly into liquid crystalline (LC) phases originally proposed to form helical chiral nematic structures (Revol et al., 1992).

However, recently Picard et al. (Picard et al., 2012) have proposed a new model in which CNCs are arranged into multilamellar smectic liquid crystals wherein each liquid plane contains nematic phases. Thus, the precise structure of CNC liquid crystalline phases is currently a topic of debate. Such LC phases can also be preserved upon air-drying to produce iridescent solid films. The LC phase of cellulose nanocrystals is sensitive to processing conditions (Pan et al., 2010) and has been exploited as a template to create novel solid-state materials containing periodic nanostructures with tunable optical properties (MacLachlan et al., 2011; Shopsowitz et al., 2012; Shopsowitz et al., 2010). Additionally, a number of patents have been filed which describe methods for incorporating patterns (Beck et al., 2010b) and controlling the iridescent wavelength (Beck et al., 2010a) of cellulose nanocrystal films by differential heating and ultrasound/high shear, respectively. Proposed applications of such films include coatings for security and optical authentication devices.

A major disadvantage of cellulose nanocrystal films is their tendency to be brittle and have poor flexibility, which is an important feature for practical applications in most fields. Mixing aqueous dispersions of CNCs with appropriate water-soluble polymers or monomers offers a possible solution, however partial loss of liquid crystalline ordering of CNCs is evident at high concentrations of additives. Zou et al. (Zou et al., 2010) demonstrated flexible and iridescent cellulose nanocrystals films by adding up to 25% wt. poly(vinyl alcohol) with low molecular weight. Recently, Tatsumi et al. (Tatsumi et al., 2012) have developed poly(2-hydroxyethyl methacrylate) (PHEMA) nanocomposites reinforced with 5 % wt. cellulose nanocrystals which have been locked in their liquid crystalline assembly via *in-situ* polymerization of HEMA. Khelifa et al. (Khelifa et al., 2012) also highlighted interesting optical properties of nanocomposites based on an acrylic copolymer matrix bearing epoxy moieties loaded with 20% wt. CNCs, which was ascribed to the formation of LC phases. Other notable works have focused on the use of external forces to produce anisotropic nanocomposites of CNCs, such

as a magnetic field (Pullawan et al., 2012) and compression molding (Rusli et al., 2010). Although, to date, 'freezing' the liquid crystalline assembly of cellulose nanocrystals into free-standing films by the addition of thermosetting epoxy monomers in aqueous media has not been reported.

In this work, we demonstrate a simple method for producing a new class of liquid crystalline thermosets based on lyotropic liquid crystals, *i.e.* cellulose nanocrystals, and water-soluble non-mesogenic epoxy monomers. These LCTs were produced by totally aqueous processing methods and ultimately cured at elevated temperatures to produce ordered networks of 'frozen' LC phases. Films were produced by casting cellulose nanocrystal/monomer mixtures from aqueous dispersions at ambient conditions and subsequent curing at elevated temperatures. X-ray diffraction experiments highlighted the effects of texture of CNCs within LCT films as compared to lyophilized CNCs. These cellulose-based LCTs exhibited thermo-mechanical properties which uniquely combined those of traditional LCTs and LCEs. All of the processed LCT films exhibited various degrees of birefringence as observed by polarized optical microscopy. In addition, the LCT films selectively attenuated the entire spectrum of UV wavelengths. Microscopic and highly localized domains of oriented cellulose nanocrystals were confirmed by transmission electron microscopy. The development of liquid crystalline thermosets based on cellulose nanocrystals and aqueous processing methods is expected to open renewable pathways for designing high performance composites with ordered network structures and unique optical properties.

Materials and Methods

Materials

Sulfuric acid (95%) and acetone (99%) were purchased from VWR Scientific (Helsinki, Finland). Dialysis tubing cellulose membrane (MWCO 12,400), 1,4-butanediol diglycidyl ether (BDGE), 2,2'-(ethylenedioxy)bis(ethylamine) (EBEA) were all purchased from Sigma-Aldrich (Helsinki, Finland).

Preparation of cellulose nanocrystals (CNCs)

CNCs were obtained from cotton fibers by acid hydrolysis with 65 wt% aqueous sulfuric acid solution (45 °C, 45 minutes). The resulting dispersion was diluted and filtered into ~200 g ice cubes and washed with distilled water until neutral pH by successive centrifugations at 12,000 rpm at 4 °C for 20 minutes. Finally, dialysis for one week against distilled water with a 12,400 MWCO dialysis membrane was performed to remove trace amounts of residual sulfuric acid. Concentrations of the resulting CNCs dispersions were calculated gravimetrically to be 3.11% wt. CNCs utilized to make LCT films were in the acid form with a solution pH = 5.9.

Film casting

Aqueous dispersions of cellulose nanocrystals (3.11% wt.) were combined with stoichiometric mixtures of 1,4-Butanediol diglycidyl ether (BDGE) (epoxy resin) and 2,2´-(Ethylenedioxy)bis(ethylamine) (EBEA) (diamine hardener). For simplicity, the molar ratio of epoxy resin to diamine hardener was kept at 1:1. The three components were stirred for 30 min at room temperature and then poured into polystyrene Petri dishes (50 mm). The films were casted by slow solvent evaporation under ambient conditions for four days. At this point, the films were initially cured at 60 °C for 24 hours, carefully removed from the polystyrene dishes, and finally cured at 150 °C in a vacuum oven for 1 hour. The resulting LCT films were calculated to contain 50-72 % wt. (or ~42-66 % v/v) CNCs. A neat epoxy film was also prepared under the same conditions for comparison.

144

145 *Atomic Force Microscopy (AFM)*

146 CNC dispersions were diluted to the desired concentration and spin-coated onto UV-treated silicon
147 wafers with an anchoring polymer at 4000 rpm. The deposition of the suspension was performed on a
148 substrate that was then spun for 30 seconds. The surfaces were then dried at 80 °C for 1 hour. The
149 spin-coated CNC films were imaged using a scanning probe microscope (model Multimode Nanoscope
150 IIIa, Digital Instruments) in tapping mode, which was equipped with an E or J scanner and with non-
151 coated silicon-etched probes (model LTESP, Veeco) with a nominal spring constant of 48 N/m.

152

153 *Attenuated Total Reflectance-Fourier Transform Infrared Spectroscopy (ATR-FTIR)*

154 Infrared spectra were obtained in order to confirm the polymerization of epoxy monomers in the
155 presence of CNCs. Dried samples were directly analyzed in a Mattson 3000 FTIR spectrometer
156 equipped with a Pike Technologies GladiATR accessory. All spectra were collected with a 2 cm^{-1}
157 resolution after 32 continuous scans.

158

159 *Differential Scanning Calorimetry*

160 Differential scanning calorimetry (DSC) was performed using a Mettler Toledo Star DSC 821e. In a
161 typical experiment *ca*. 10 mg of dry sample was placed in the DSC cell and first heated from -50 to 200
162 °C, followed by a second ramp from -50 to 225 °C (heating rate of 10 °C min^{-1}). The glass transition
163 temperature T_g and change in heat capacity ΔC_p were calculated from the second heating cycle using
164 Mettler Toledo STARe software.

165

166 *Dynamic Mechanical Analysis*

DMA measurements were performed using a DMA Q800 with rectangular films (*ca*. 10 x 5.5 x 0.35 mm) in tensile mode with an oscillation frequency of 1 Hz, a static force of 10 mN, and an oscillation amplitude of 5 µm. Measurements were carried out at a heating rate of 3 °C min^{-1} in the temperature range of -100 to 150 °C. Tensile tests of films were also carried out at 35 °C under 3 N/min isothermal ramp. All measurements were performed at ambient humidity. Rectangular sample sections were taken from the centers of each film for consistency between measurements.

UV/Vis-spectrophotometer

Ultraviolet-visible spectroscopy was conducted on a UNICAM HELIOS β UV/Vis spectrophotometer. Transmission spectra of the samples in the wavelength range of 190 nm to 1000 nm were collected by mounting free-standing LCT films so that the surfaces of the films were perpendicular to the beam path.

Polarized optical microscopy

Optical birefringence of LCT films was visualized with an Olympus BH-2 microscope equipped with a full-wave retardation plate and Nikon Coolpix 990 digital camera. All images were taken with the polarizer and analyzer in a crossed (orthogonal) arrangement at low magnification, *i.e.* zoom lens 5X and 10X. All photographs were taken with the same illumination conditions and exposure time.

X-ray Diffraction (XRD)

XRD experiments were carried out at ambient temperature on freeze-dried CNCs, a pure CNC film and LCT films in powder mode. Samples of freeze-dried CNCs were prepared by powder placement in the sample holder and manually pressing with a flat plate, while flexible LCT films were simply placed in

the sample holder. A PANalytical X'Pert PRO MPD diffractometer operated with a CuK_α anode (λ = 0.154 nm) in parallel geometry was used with a 2θ range from 5° to 40° with steps of 0.0263° and a scanning speed of 2.67°/min. The crystallinity index (*CrI*) was calculated by the method of Segal et al. (Segal et al., 1959) according to:

$$CrI = 1 - \frac{I_{am}}{I_{200}},$$

where I_{200} is the maximum intensity (arbitrary units) of the (200) lattice diffraction and I_{am} is the intensity of diffraction (in the same units) at 2θ = 18°.

The dimension of the crystal D_{hkl} was evaluated from a Lorentzian peak function of the (200) lattice diffraction by using Scherrer's formula (Klug and Alexander, 1954):

$$D_{hkl} = \frac{0.9 \times \lambda}{\beta_{1/2} \times \cos\theta},$$

where θ is the diffraction angle, λ the X-ray wavelength and $\beta_{1/2}$ the peak width at half of maximum intensity.

Transmission Electron Microscopy

LCT films were sectioned using a microtome and deposited on copper mesh grids and observed with a JEOL JEM-3200FSC transmission electron microscope (TEM) operated at an accelerating voltage of 200 kV.

Results and Discussion

Preparation of cellulose nanocrystals and liquid crystalline thermosets

To date, most efforts to produce epoxy nanocomposites containing cellulose nanocrystals have been focused on their use as matrix reinforcement up to *ca*. 24 % (v/v) (Ruiz et al., 2000; Ruiz et al., 2001; Rusli and Eichhorn, 2008, 2011; Tang and Weder, 2010). Contrarily, the objective of this work was to produce liquid crystalline thermosetting (LCT) films using cellulose nanocrystals as the primary mesogenic component by the addition of water-soluble non-mesogenic epoxy precursors. To this effect, cellulose nanocrystals were produced from cotton fiber by sulfuric acid hydrolysis to form highly stable aqueous dispersions. The resulting CNCs were determined to have widths ranging ~4-12 nm and lengths from ~100-200 nm according to AFM height images (see Fig. S1 in Supplementary data), which were comparable to recent literature (Habibi et al., 2010).

It is widely known that CNCs spontaneously self-assemble into liquid crystalline phases at a specific range of concentrations, which depends on their aspect ratio (Habibi et al., 2010; Moon et al., 2011; Picard et al., 2012; Revol et al., 1992) as dictated by the Onsager theory of colloidal liquid crystals (Onsager, 1949). The LC phase is preserved upon slow evaporation of water to produce iridescent films with tunable optical properties (Picard et al., 2012; Revol et al., 1998). However, CNC films are typically brittle which provides a challenge for their use in practical applications. In an effort to produce CNC films which preserve their LC assembly and introduce flexibility, a water-soluble epoxy monomer, 1,4-butanediol diglycidyl ether (BDGE), and a diamine hardener, 2,2'-(ethylenedioxy)bis(ethylamine) (EBEA) were mixed with aqueous dispersions of CNCs. The mixtures were film casted in polystyrene dishes by slow solvent evaporation over about four days. Once the films were dry, they were partially cured at 60 ºC for 24 hours, carefully removed from the polystyrene dishes, followed by final curing at 150 ºC for 1 hour. The resulting LCT films contained between 50-72 % wt. CNCs, as calculated gravimetrically from aqueous dispersions (3.11% wt.). An attempt was made to produce LCT films containing higher compositions of CNCs, however they were too brittle to

233 be removed from the Petri dishes without rupturing. A neat epoxy film was also prepared by mixing the
234 epoxy monomer with diamine hardener and casting, following the same curing schedule.

235 To confirm the curing reaction between the epoxy monomer and diamine hardener in the
236 presence of CNCs, the LCT films were characterized by ATR-FTIR spectroscopy. Shown in Figure 1
237 are FTIR spectra of lyophilized CNCs, neat epoxy film, and the highest (72 % wt.) and lowest (50 %
238 wt.) CNC compositions of LCT films. All other LCT films displayed similar spectra and for simplicity
239 are not shown here. As compared to lyophilized CNCs, typically the LCT films showed changes in
240 peak intensities in the range from 1500-1000 cm^{-1}, which corresponded to various C-O bonds present
241 in the cured epoxy. Characteristic peaks corresponding to an epoxide ring (950-900 cm^{-1}) were slightly
242 overlapped by the cellulose spectrum such that its presence could not be accurately detected.
243 Additionally, the most obvious peak appeared at 1650 cm^{-1} and corresponded to a secondary amine (N-
244 H) bending vibration of the cured epoxy in the LCT film. The same characteristic peak at 1650 cm^{-1}
245 was also observed in a neat cured epoxy film, which confirmed success of the curing reaction in the
246 presence of CNCs.

247

248 *Optical properties*

249 The resulting LCT films were easily removed and flexible, however they were not iridescent as
250 compared to pure CNC films by the naked eye. Also, slight darkening of LCT films was evident which
251 was attributed to the presence of acidic sulfate groups on CNCs surfaces as shown in the small inset of
252 Figure 2. The films were 300-400 μm thick, and noted to be slightly thicker near the center. Since the
253 LCT films were casted from water in polystyrene dishes, the variations in film thickness were likely
254 due to a complex synergy between surface energy phenomena associated with water droplet
255 evaporation from hydrophobic surfaces (Picknett and Bexon, 1977), the “coffee ring effect” (Uetani

and Yano, 2012) and the intermolecular interactions of epoxy monomers with CNCs. This may have caused heterogeneous distributions of epoxy monomers and CNCs within LCT films, thus variations in film thickness. When viewed under crossed-polarizers, the entirety of all the LCT films displayed some degree of birefringence, but brilliant color patterns spanning the visible spectrum were observed predominantly near the film edges, as shown in Figure 2a. On the other hand, away from the film edges, variations such as brighter (Figure 2b) and darker areas (Figure 2c) were observed under crossed-polarizers. A neat epoxy film showed no birefringence as indicated by complete lack of light transmittance when viewed between crossed-polarizers (not shown here). This was an indication that the cured epoxy resin alone was isotropic, such that any birefringence observed in LCT films was derived from orientations caused by the presence of CNCs.

The birefringence observed near LCT film edges was similar to that of locally oriented anisotropic glass as previously described for CNCs cast under vacuum (Viet et al., 2007). However, variations in film thickness may have resulted from heterogeneous distributions of CNCs and cured epoxy within the LCT films, thus significant differences in color patterns and overall birefringence was observed. For example, the darker textures, such as in Figure 2c, indicated optically isotropic areas such that low concentrations of oriented CNCs and high concentrations of cured epoxy were present. These findings indicated that opportunities might exist to fine tune the optical properties of cellulose-based LCT films by varying the processing conditions (Beck et al., 2010a, b). The observed birefringence would suggest that CNCs were able to self-assemble into oriented phases more effectively at the film edges, possibly due to lower concentrations of non-mesogenic epoxy monomers during solvent evaporation. However, the fingerprint texture characteristic of CNCs periodic liquid crystalline structure was not observed. A pure CNC film cast under similar conditions, shown in Figure 2d, displayed typical color textures arising from their periodic LC structures (Picard et al., 2012; Revol

et al., 1998), but these characteristics were not observed for any of the LCT films. Evidently, the presence of non-mesogenic epoxy monomers disrupted the formation of periodic LC phases during the solvent evaporation process. Overall, the observed birefringence of LCT films, although heterogeneous, gave indirect evidence for CNCs assembled into various domains of oriented phases, which was later confirmed by transmission electron microscopy.

The 'frozen' LC phases present in iridescent CNC films is known to cause specific attenuations in the visible region of the electromagnetic spectrum, which has been associated with the helical pitch of chiral nematic structures (Shopsowitz et al., 2010). However, Picard et al. (Picard et al., 2012) would argue that such attenuations are associated with lamella thickness of smectic phases and explained by classical light interference. UV-Vis spectra of a pure CNC film, neat epoxy film, and the highest (72 % wt.) and lowest (50 % wt.) CNC compositions of LCT films are shown in Figure 3. All other LCT films displayed similar UV spectra and for simplicity are not shown here. In this case, pure CNC films gave an attenuation peak at ~600 nm. In contrast, the neat epoxy film and LCT films did not show a peak, which suggested a lack of periodic LC structure. The neat epoxy film was semi-transparent (~60-70 % transmittance) in the visible region, while LCT films were only transparent at higher wavelength ranges approaching near infrared. Nevertheless, the presence of CNCs in the LCT films yielded a ~100 nm redshift, which led to selective attenuation of the entire UV wavelength range. This was most likely due to the slight darkening of LCT films as shown in the inset of Figure 2. Nevertheless, these results suggested that LCT films could also be useful as functional composites that require UV attenuation, having similar properties to cellulose composites that incorporated TiO_2 nanoparticles as UV absorbers (Zhou et al., 2006).

Cellulose degree of crystallinity

X-ray diffraction measurements were carried out to determine cellulose degree of crystallinity and reveal the effects of texture of CNCs within LCT films. Shown in Figure 4 are the XRD spectra of the four LCT films produced containing 50-72 % wt. CNCs, a neat epoxy film, a pure CNC film and a sample of lyophilized CNCs. As expected, the neat epoxy film did not show any diffraction peaks in the 2θ = 5-40º range, which indicated a completely amorphous material. Samples of lyophilized CNCs showed the typical XRD spectrum for cellulose I (Nishiyama et al., 2002; Park et al., 2010), displaying 2θ diffraction peaks at 14.8 (1-10), 16.5 (110), 22.8 (200) and 34.5° (004). The same diffraction peaks were observed in all of the LCT films, although notable differences in peak intensities were observed, especially in peaks from (1-10) and (110) reflections. In the case of lyophilized CNCs, which were thought to be preferentially oriented along the nanocrystal axis by mechanical pressing (Klug and Alexander, 1954), the peak intensities for (1-10) and (110) reflections were relatively low compared to (200). However, a notable increase in intensity for (1-10) relative to the (110) and (200) reflections was observed for all the LCT films, presented in Table 1 as an intensity ratio ($I_{200}/I_{1\text{-}10}$). This suggested that while lyophilized CNCs existed with a preferred axial orientation (along the fiber axis) (Klug and Alexander, 1954; Yoshiharu et al., 1997), this effect progressively decreased for CNCs in LCT films as indicated by more intense (1-10) reflections relative to (200) in Figure 4. A pure and iridescent CNC film was also analyzed to confirm the differences in peak intensities due to preferred orientation (top of Figure 4). The pure CNC film, which is known to contain periodic LC phases (Picard et al., 2012) (see Figure 2d), displayed a similar increase in the (1-10) reflection relative to (200). Even though pure CNC films were highly ordered into periodic phases, their domains were too small to be detected by XRD (Yoshiharu et al., 1997). It has been proposed that CNC periodic phases contain differently shaped bundles of CNCs within different lamella (Picard et al., 2012), and the precise arrangement of CNCs within each bundle is unknown. On the other hand, the traditional chiral nematic model of CNCs

(Revol et al., 1992) provides precise helicoidal arrangements. The results of XRD indicate here that the overall microstructure of pure CNC films appeared more isotropic (randomly oriented) as compared to lyophilized CNCs. This suggested that CNCs in LCT films were oriented along many different directors, which could partially explain the overall apparent lack of texture compared to lyophilized CNCs. While these findings were not taken as evidence of periodic LC phases in LCT films, the significant changes in relative peak intensities compared to lyophilized CNCs highlighted the importance of texture on routine interpretations of XRD spectra of cellulose (Park et al., 2010).

From the XRD spectra, the intensity ratio ($I_{200}/I_{1\text{-}10}$), crystallinity indices and average crystallite widths were calculated based on Scherrer's formula with a shape constant of 0.9 (Klug and Alexander, 1954), and are summarized in Table 1. Lyophilized cotton CNCs gave a crystallinity index of 90.7 % and crystallite width of 6.6 nm, which was in good agreement with AFM images (see Fig. S1 in Supplementary data). The crystallinity index and crystallite width of CNCs within the LCT films generally increased with increasing amount of CNCs. Interestingly, LCT films gave much higher crystallinity indices than would have been expected based on the film compositions. For example, LCT films containing only 50% wt. CNCs gave a crystallinity index of 85.1 %, which was only ~5 % less than pure lyophilized CNCs. In addition, the average crystallite width showed slight increases as the CNC composition of LCT films was increased, up to 7.0 nm, however this was considered to be within experimental error given the textural effects observed in Figure 4. The pure and iridescent CNC film displayed a crystallinity index of 85.6 %, which was surprisingly lower than lyophilized CNCs. Indeed, the Scherrer method assumes that crystallites are randomly oriented (Klug and Alexander, 1954), and preferred orientation of crystallites is known to affect peak intensity and broadening. Thus, calculations of crystallinity index and crystallite dimensions were believed to be affected by differences in overall orientation of cellulose crystallites in the films. Also, the method of Segal et al. (Segal et al., 1959) to

calculate the crystallinity index (*CrI*) from XRD spectra has been known to overestimate cellulose degree of crystallinity as compared to other methods, such as solid-state ^{13}C-NMR (Park et al., 2010). It is important to note that the calculations of crystallinity index (*CrI*) from XRD spectra only provided an empirical measure of relative cellulose degree of crystallinity.

The intensity ratio of the (200) and (1-10) reflections, ($I_{200}/I_{1\text{-}10}$), was calculated from XRD spectra as a qualitative comparison of textural effects between CNC samples. For lyophilized CNCs, the ratio ($I_{200}/I_{1\text{-}10}$) was the highest and assumed to be due to preferred axial orientation of crystallites by mechanical pressing (Klug and Alexander, 1954). Interestingly, the intensity ratio ($I_{200}/I_{1\text{-}10}$) for LCT films displayed a trend based on the film compositions, such that as the concentration of CNCs was increased, the intensity ratio ($I_{200}/I_{1\text{-}10}$) decreased. This indicated that the overall preferred axial orientation of CNCs became less pronounced at higher concentrations. The pure and iridescent CNC film showed the lowest ratio ($I_{200}/I_{1\text{-}10}$), which correlated well with the trend observed for LCT films. As previously noted, the relative peak intensities were not taken as an indication of periodic LC structures, however the variations in peak intensities between samples highlighted the importance of preferred orientation on routine interpretations of XRD spectra of cellulose (Park et al., 2010).

Thermo-mechanical properties

Besides the unique optical properties exhibited by epoxy-based liquid crystalline thermosets (Amendola et al., 1996; Tan and Fung, 2001), desirable thermo-mechanical properties such as increased modulus and fracture toughness are expected to result from their highly ordered networks (Barclay and Ober, 1993; Carfagna et al., 1997; Kannan and Sudhakara, 2011; Ortiz et al., 1998a). Thermal transitions of LCT films were initially observed by DSC and the results are summarized in Table 2. Samples of lyophilized CNCs, LCT films and a neat epoxy film were first subjected to a

371 temperature ramp from -50 to 200 °C, followed by a second cycle from -50 to 225 °C. The first
372 temperature cycle was only brought to 200 °C so to avoid any thermal degradation of cellulose. After
373 removal of thermal history, lyophilized CNCs showed a glass transition (T_g) of 211 °C, in good
374 agreement with other highly crystalline forms of cellulose I (Szczesniak et al., 2008). Contrarily, it was
375 clear that the only thermal transition that could be observed in LCT films was the glass transition (T_g)
376 of the cured epoxy resin. The glass transition of cellulose is highly dependent on degree of crystallinity,
377 moisture content and thermal history, such that the T_g of CNCs within LCT films could not be
378 observed. The pure amorphous epoxy film showed a T_g of -21.9 °C, while the T_g's of LCT films were
379 insignificantly decreased by ~1-2 °C. Due to the low epoxy content of the LCT film containing 72 %
380 wt. CNCs, no thermal transitions were observed. From the glass transitions, changes in heat capacity,
381 ΔC_p, were also determined from each sample and correlated to the film compositions. As shown in
382 Table 2, the experimentally determined compositions of the LCT films followed a reasonable trend in
383 correlation with the stoichiometric values, based on initial content of aqueous dispersions. However,
384 the inherent heterogeneities and variations in LCT film thickness may have caused some deviation in
385 the experimentally determined compositions.

386 Typically, pure CNC films are very brittle and challenging for dynamic mechanical analysis
387 (Bras et al., 2011), thus CNC stiffness and deformation have been determined within epoxy
388 nanocomposites by techniques such as Raman spectroscopy (Rusli and Eichhorn, 2008, 2011; Sturcova
389 et al., 2005). In this case, we obtained flexible LCT films containing up to 72 % wt. CNCs which were
390 highly durable for mechanical analysis. Rectangular sample sections were taken from the center of each
391 LCT film for consistent analysis between samples. The evolution of storage modulus (E') of LCT films
392 and neat epoxy was monitored over a temperature range of -100 to 150 ºC by Dynamic Mechanical
393 Analysis (DMA), shown in Figure 5(a). As compared to the neat epoxy film, all of the LCT films

exhibited significantly higher moduli over the entire temperature range. This was expected since the LCT films contained cotton cellulose nanocrystals as the major component, which have a reported theoretical modulus between 57-105 GPa (Rusli and Eichhorn, 2008). Additionally, all the LCT films were mechanically stable up to the onset of thermal degradation of CNCs at ~225 ºC (data not shown here). In the glassy state, LCT films showed roughly constant modulus (E') values *i.e.* 11-18 GPa, compared to ~2 GPa for the neat epoxy film. The observed glass transitions (T_g) of the epoxy resins at about -25 °C were in good agreement with the results of DSC (Table 2). After the glass transition of the neat epoxy film, the storage modulus decreased to a minimum ($E' < 1$ MPa) as the temperature reached ambient conditions. Similarly, the LCT films displayed glass transitions between -30 and -20 ºC, but held storage moduli (E') between 300 MPa to 1 GPa at ambient conditions depending on composition. The LCT films also showed slight increases in modulus at higher temperatures, likely caused by additional curing of secondary amines (Ortiz et al., 1998a). Overall, trends in the evolution of storage modulus were similar for all LCT films regardless of the CNCs composition. Nevertheless, it appeared that increased amounts of CNCs in LCT films resulted in increased storage modulus, especially at the high temperature range (> 100 ºC). Given that CNCs were the primary component of the LCT films, and well above their percolation threshold (Bras et al., 2011), a highly percolated anisotropic network was the most likely cause for the observed mechanical stability. Overall, it was concluded that LCT films gave desirable thermo-mechanical properties compared to pure CNC films which were too brittle for dynamic mechanical analysis and gave up to a 1000-fold increase in storage modulus (E') compared to the neat epoxy film at ambient conditions.

Traditional LCTs, which incorporate 'frozen' thermotropic liquid crystals, exhibit high glass transitions temperatures (T_g > 150 ºC) and high moduli (E ~1 GPa) at room temperature (Barclay and Ober, 1993; Ortiz et al., 1998a; Shiota and Ober, 1997). On the other hand, liquid crystalline

417 elastomers (LCEs) are more loosely cross-linked networks exhibiting low glass transitions (T_g < 35 ºC)
418 and low moduli (E < 1 MPa) at room temperature (Giamberini et al., 2005; Ortiz et al., 1998b; Ribera
419 et al., 2006). In the latter case, liquid crystalline phase transitions are also observed due to high
420 mobility of mesogens within the network. Since cellulose nanocrystals are lyotropic, the presence of a
421 suitable solvent, in most cases water, is a prerequisite to observe liquid crystalline phase transitions
422 (Habibi et al., 2010; Moon et al., 2011). The LCT films produced in this work were via slow
423 evaporation of water, thus, once dried and cured, CNCs existed in a 'frozen' state similar to traditional
424 LCTs. It is important to note that in the case of traditional LCEs and LCTs, mesogens are usually
425 covalently cross-linked within the polymeric network, but in this case, LCT films consisted primarily
426 of non-cross-linked CNCs within a secondary non-mesogenic epoxy network. Interestingly, these
427 cellulose-based LCT films uniquely exhibited thermo-mechanical properties of both classes of cross-
428 linked liquid crystalline networks. Although they displayed very low glass transition temperatures, *i.e.*
429 -25 ºC, thus existed in the rubbery state at room temperature similar to LCEs, they also displayed high
430 moduli similar to LCTs, *i.e.* from 300 MPa to 1 GPa (see Figure 5(a)). Of course, the results of DSC
431 (Table 2) showed that pure CNCs had a glass transition (T_g) of 211 °C, but this could not be observed
432 in the LCT films. This demonstrated that cellulose nanocrystals have a unique advantage as the
433 mesogenic components of LCTs, due to their combined high modulus, high T_g and 'frozen' LC phases
434 within solid films.

435 The results of DMA measurements were also confirmed by nonlinear deformation (stress vs.
436 strain) experiments conducted on LCT and neat epoxy films at ambient conditions. Typical stress-strain
437 curves are shown in Figure 5(b), in which the insert displays the same example curves from 0 to 8 %
438 strain. The neat epoxy film showed behavior more typical of an elastomer, exhibiting low elastic
439 modulus (E < 1 MPa), very low tensile strength and high elongation at break, *i.e.* ~40 %. Contrarily,

440 the LCT films showed significantly higher modulus and lower elongation at break. Typical elastic
441 moduli (*i.e.* Young's modulus) of the LCT films derived from the linear portion of the stress-strain
442 curve were from 700 MPa to 1.5 GPa depending on the CNCs composition, and were in reasonable
443 agreement with results of the dynamic mechanical measurements (Figure 5(a)). Also, the elongation at
444 break of LCT films was typically from 2 to 8 %, with ultimate tensile strengths from 5 to 7 MPa. These
445 values were found to be comparable to other types of epoxy LCTs based on thermotropic liquid
446 crystals, even though most traditional epoxy LCTs display much higher glass transitions, thus exist in
447 the glassy state at room temperature (Kannan and Sudhakara, 2011). As compared to epoxy-based
448 LCEs (Giamberini et al., 2005; Ortiz et al., 1998b; Ribera et al., 2006), similar, if not significantly
449 enhanced, modulus values were observed in the cellulose-based LCT films. As mentioned previously,
450 the results of DSC (Table 2) showed that pure CNCs had a glass transition (T_g) of 211 °C, but this
451 could not be observed in the LCT films. In general, it appeared that with high content of CNCs, LCT
452 films exhibited increased elastic modulus, but decreased elongation at break. As previously discussed,
453 CNCs were the primary component of the LCT films, and well above their percolation threshold (Bras
454 et al., 2011), thus a highly percolated anisotropic network was the most likely cause for the observed
455 mechanical stability. The mechanical properties of pure CNC films were very difficult to analyze due
456 to their brittleness. Nevertheless, tensile tests have been successfully performed by Bras et al. on a
457 variety of CNC films from different cellulose sources, in which the experimental elastic modulus (E) of
458 2.13 GPa was determined for a cotton CNC film. This appeared to be in good agreement with the
459 results of our tensile tests. The mechanical properties, such as elastic modulus (E), of LCT films based
460 on CNCs were also increased in comparison to previous studies of epoxy nanocomposites (Ruiz et al.,
461 2000; Ruiz et al., 2001; Rusli and Eichhorn, 2011; Tang and Weder, 2010). This was expected due to
462 the high compositions of CNCs within LCT films (up to 72 % wt.) as compared to previous epoxy

nanocomposites which only contained up to 24 % (v/v) CNC reinforcement. In general, LCT films based on renewable cellulose nanocrystals were strong and highly durable, which may provide better use for practical applications.

Electron Microscopy

In order to visualize the microstructure of LCT films, images were obtained from thinly sliced sections by transmission electron microscopy (TEM). Sections were taken from various areas of four different films to confirm the optical heterogeneities observed by polarized light microscopy (Figure 2). Shown in Figure 6 are typical examples of textures obtained from LCT films at (a) the edges and (b) near the center. Interestingly, as seen in Figure 6(a), the textures at the film edges appeared to show large microscopic domains of oriented CNCs, as opposed to small and localized domains near the film center, shown in Figure 6(b). The observed textures at film edges were consistent between four samples therefore was not likely an artifact due to sample preparation (microtome). Similar LC phases have been observed in the case of solid films of self-assembled CdSe nanorods (Li and Alivisatos, 2003; Talapin et al., 2004). As mentioned previously, the heterogeneities in LCT film microstructure were likely due to a complex synergy between surface energy phenomena associated with water evaporation from hydrophobic surfaces (Picknett and Bexon, 1977), the "coffee ring" effect (Uetani and Yano, 2012) and the intermolecular interactions of epoxy monomers with CNCs. The "coffee ring" effect has been utilized to analyze CNC anisotropic structures, in which highly oriented phases occurred at the ring perimeter of evaporated water droplets. Also, since the LCT films were noted to have higher thickness near the center, it was likely that higher concentrations of cured epoxy were present, such that CNCs were able to self-assemble into oriented phases more effectively at the film edges with less disruption from non-mesogenic epoxy monomers. There was no evidence of CNCs assembled into

periodic LC phases as observed in pure cellulose nanocrystal films (Picard et al., 2012; Revol et al., 1992), which were likely disrupted by the presence of non-mesogenic epoxy monomers. Nevertheless, the nanostructures shown in Figure 6 confirmed highly localized and microscopic domains of oriented CNCs within the LCT films. The noted structural differences between various locations of LCT films were further evidence that by varying the processing conditions, CNCs liquid crystalline phases could potentially be fine-tuned. This conclusion was supported by the birefringence patterns observed by polarized optical microscopy (Figure 2) and the different reflection intensities of XRD spectra (Figure 4) for LCT films.

Conclusions

A new class of liquid crystalline thermosets (LCTs) was successfully produced containing lyotropic cellulose nanocrystals as the primary mesogenic component by the addition of non-mesogenic epoxy monomers. These LCTs were produced by totally aqueous processing methods and ultimately cured at elevated temperatures to produce ordered networks of 'frozen' liquid crystalline phases. X-ray diffraction experiments highlighted the effects of texture of cellulose nanocrystals within LCT films compared to the lyophilized state. All of the processed films exhibited various degrees of birefringence depending on location as observed by polarized optical microscopy. These findings indicated that opportunities might exist to fine tune the optical properties of cellulose-based LCT films by varying the processing conditions. In addition, the LCT films selectively attenuated UV wavelengths. These cellulose-based LCTs exhibited highly desirable thermo-mechanical properties and flexibility compared to neat cellulose nanocrystal films, which were too brittle for dynamic mechanical analysis. Interestingly, these cellulose-based LCT films uniquely exhibited thermo-mechanical properties of both classes of cross-linked liquid crystalline networks, namely liquid crystalline

thermosets (LCTs) and liquid crystalline elastomers (LCEs). Although they displayed very low glass transition temperatures (~ -25 °C), thus existed in the rubbery state at room temperature similar to LCEs, they also displayed high moduli (~1 GPa) similar to LCTs. Pure CNCs showed a glass transition (T_g) of 211 °C, but this was not observed in the LCT films. This demonstrated that cellulose nanocrystals have a unique advantage as the mesogenic components of LCTs, due to their combined high modulus, high T_g and 'frozen' LC phases within solid films. The self-assembly of cellulose nanocrystals into microscopic and highly localized domains of oriented phases was confirmed by transmission electron microscopy. The development of liquid crystalline thermosets based on cellulose nanocrystals and totally aqueous processing methods is expected to open more renewable pathways for designing high performance composites with ordered network structures and unique optical properties.

Acknowledgements

The authors wish to acknowledge Dr. Nguyen Dang Luong and Dr. Markus Valkeapää for assistance with XRD experiments. Also, the authors would like to thank Dr. Jani Seitsonen and Prof. Janne Ruokolainen for performing TEM analysis. Funding support from Aalto University and the Academy of Finland (Dec. No. 137759) are greatly appreciated.

Supplementary Data

An AFM height image of cellulose nanocrystals produced from this work is available as supplementary data.

References

Amendola, E., Carfagna, C., Giamberini, M., Komitov, L. (1996). Anisotropic liquid crystalline epoxy thermoset. *Liq. Cryst.*, *21*(3), 317-325. doi:10.1080/02678299608032840

Barclay, G. G., Ober, C. K. (1993). Liquid crystalline and rigid-rod networks. *Prog. Polym. Sci., 18*(5), 899-945. doi:10.1016/0079-6700(93)90021-4

Beck, S., Bouchard, J., Berry, R. (2010a). Control of nanocrystalline cellulose film iridescence wavelength. WO 2010124396.

Beck, S., Bouchard, J., Berry, R. (2010b). Iridescent solid nanocrystalline cellulose films incorporating patterns and their production. WO 2010066029.

Bras, J., Viet, D., Bruzzese, C., Dufresne, A. (2011). Correlation between stiffness of sheets prepared from cellulose whiskers and nanoparticles dimensions. *Carbohydr. Polym., 84*(1), 211-215. doi:10.1016/j.carbpol.2010.11.022

Brondsted, P., Lilholt, H., Lystrup, A. (2005). Composite materials for wind power turbine blades. *Annu. Rev. Mater. Res., 35*, 505-538. doi:10.1146/annurev.matsci.35.100303.110641

Carfagna, C., Amendola, E., Giamberini, M. (1994). Liquid crystalline epoxy resins. *Liq. Cryst. Polym., Proc. Int. Workshop*, 69-85

Carfagna, C., Amendola, E., Giamberini, M. (1997). PII: Liquid crystalline epoxy based thermosetting polymers. *Prog. Polym. Sci., 22*(8), 1607-1647. doi:10.1016/s0079-6700(97)00010-5

Giamberini, M., Cerruti, P., Ambrogi, V., Vestito, C., Covino, F., Carfagna, C. (2005). Liquid crystalline elastomers based on diglycidyl terminated rigid monomers and aliphatic acids. Part 2. Mechanical characterization. *Polymer, 46*(21), 9113-9125. doi:10.1016/j.polymer.2005.04.093

Habibi, Y., Lucia, L. A., Rojas, O. J. (2010). Cellulose Nanocrystals: Chemistry, Self-Assembly, and Applications. *Chem. Rev., 110*(6), 3479-3500. doi:10.1021/cr900339w

Kannan, P., Sudhakara, P. (2011). Liquid crystalline thermoset epoxy resins. *High Perform. Polym. Eng. Plast.*, 387-422. doi:10.1002/9781118171950.ch11

Khelifa, F., Habibi, Y., Benard, F., Dubois, P. (2012). Effect of cellulosic nanowhiskers on the performances of epoxidized acrylic copolymers. *J. Mater. Chem., 22*(38), 20520-20528. doi:10.1039/c2jm33917j

Klug, H. P., Alexander, L. E. (1954). *X-Ray Diffraction Procedures for Polycrystalline and Amorphous Materials*. New York: Wiley Interscience

Li, L.-S., Alivisatos, A. P. (2003). Semiconductor nanorod liquid crystals and their assembly on a substrate. *Adv. Mater. (Weinheim, Ger.), 15*(5), 408-411. doi:10.1002/adma.200390093

MacLachlan, M. J., Shopsowitz, K. E., Hamad, W. Y., Qi, H. (2011). Inorganic mesoporous materials with chiral nematic structures and preparation method thereof. WO 2011123929.

May, C. A., Tanaka, Y. (1973). *Epoxy Resins: Chemistry and Technology*. New York: Marcel Dekker

565 Moon, R. J., Martini, A., Nairn, J., Simonsen, J., Youngblood, J. (2011). Cellulose nanomaterials
566 review: structure, properties and nanocomposites. *Chem. Soc. Rev., 40*(7), 3941-3994.
567 doi:10.1039/c0cs00108b

568 Nishiyama, Y., Langan, P., Chanzy, H. (2002). Crystal structure and hydrogen-bonding system in
569 cellulose Iβ from synchrotron x-ray and neutron fiber diffraction. *J. Am. Chem. Soc., 124*(31), 9074-
570 9082. doi:10.1021/ja0257319

571 Onsager, L. (1949). The effects of shapes on the interaction of colloidal particles. *Ann. N. Y. Acad. Sci.,*
572 *51*, 627-659. doi:10.1111/j.1749-6632.1949.tb27296.x

573 Ortiz, C., Kim, R., Rodighiero, E., Ober, C. K., Kramer, E. J. (1998a). Deformation of a Polydomain,
574 Liquid Crystalline Epoxy-Based Thermoset. *Macromolecules, 31*(13), 4074-4088.
575 doi:10.1021/ma971439n

576 Ortiz, C., Wagner, M., Bhargava, N., Ober, C. K., Kramer, E. J. (1998b). Deformation of a
577 Polydomain, Smectic Liquid Crystalline Elastomer. *Macromolecules, 31*(24), 8531-8539.
578 doi:10.1021/ma971423x

579 Pan, J., Hamad, W., Straus, S. K. (2010). Parameters Affecting the Chiral Nematic Phase of
580 Nanocrystalline Cellulose Films. *Macromolecules (Washington, DC, U. S.), 43*(8), 3851-3858.
581 doi:10.1021/ma902383k

582 Park, S., Baker, J. O., Himmel, M. E., Parilla, P. A., Johnson, D. K. (2010). Cellulose crystallinity
583 index: measurement techniques and their impact on interpreting cellulase performance. *Biotechnol.*
584 *Biofuels, 3*(10), No pp given. doi:10.1186/1754-6834-3-10

585 Picard, G., Simon, D., Kadiri, Y., LeBreux, J. D., Ghozayel, F. (2012). Cellulose Nanocrystal
586 Iridescence: A New Model. *Langmuir, 28*(41), 14799-14807. doi:10.1021/la302982s

587 Picknett, R. G., Bexon, R. (1977). The evaporation of sessile or pendant drops in still air. *J. Colloid*
588 *Interface Sci., 61*(2), 336-350. doi:10.1016/0021-9797(77)90396-4

589 Pullawan, T., Wilkinson, A. N., Eichhorn, S. J. (2012). Influence of Magnetic Field Alignment of
590 Cellulose Whiskers on the Mechanics of All-Cellulose Nanocomposites. *Biomacromolecules, 13*(8),
591 2528-2536

592 Retegi, A., Algar, I., Martin, L., Altuna, F., Stefani, P., Zuluaga, R., Ganan, P., Mondragon, I. (2012).
593 Sustainable optically transparent composites based on epoxidized soy-bean oil (ESO) matrix and high
594 contents of bacterial cellulose (BC). *Cellulose (Dordrecht, Neth.), 19*(1), 103-109. doi:10.1007/s10570-
595 011-9598-8

596 Revol, J. F., Bradford, H., Giasson, J., Marchessault, R. H., Gray, D. G. (1992). Helicoidal self-
597 ordering of cellulose microfibrils in aqueous suspension. *Int. J. Biol. Macromol., 14*(3), 170-172.
598 doi:10.1016/s0141-8130(05)80008-x

599 Revol, J. F., Godbout, L., Gray, D. G. (1998). Solid self-assembled films of cellulose with chiral
600 nematic order and optically variable properties. *J. Pulp Pap. Sci., 24*(5), 146-149

601 Ribera, D., Giamberini, M., Serra, A., Mantecon, A. (2006). Lightly crosslinked, mesomorphic
602 networks obtained through the reaction of dimeric, liquid-crystalline epoxy-imine monomers and
603 heptanedioic acid. *J. Polym. Sci., Part A Polym. Chem., 44*(21), 6270-6286. doi:10.1002/pola.21681

604 Ruiz, M. M., Cavaille, J. Y., Dufresne, A., Gerard, J. F., Graillat, C. (2000). Processing and
605 characterization of new thermoset nanocomposites based on cellulose whiskers. *Compos. Interfaces,*
606 *7*(2), 117-131

607 Ruiz, M. M., Cavaille, J. Y., Dufresne, A., Graillat, C., Gerard, J.-F. (2001). New waterborne epoxy
608 coatings based on cellulose nanofillers. *Macromol. Symp., 169*(Fillers and Filled Polymers), 211-222.
609 doi:10.1002/1521-3900(200105)169:1<211::aid-masy211>3.0.co;2-h

610 Rusli, R., Eichhorn, S. J. (2008). Determination of the stiffness of cellulose nanowhiskers and the fiber-
611 matrix interface in a nanocomposite using Raman spectroscopy. *Appl. Phys. Lett., 93*(3),
612 033111/033111-033111/033113. doi:10.1063/1.2963491

613 Rusli, R., Eichhorn, S. J. (2011). Interfacial energy dissipation in a cellulose nanowhisker composite.
614 *Nanotechnology, 22*(32), 325706/325701-325706/325708. doi:10.1088/0957-4484/22/32/325706

615 Rusli, R., Shanmuganathan, K., Rowan, S. J., Weder, C., Eichhorn, S. J. (2010). Stress-Transfer in
616 Anisotropic and Environmentally Adaptive Cellulose Whisker Nanocomposites. *Biomacromolecules,*
617 *11*(3), 762-768. doi:10.1021/bm1001203

618 Segal, L., Creely, J. J., Martin, A. E., Conrad, C. M. (1959). An empirical method for estimating the
619 degree of crystallinity of native cellulose using the X-ray diffractometer. *Text. Res. J., 29*, 786-794

620 Shimazaki, Y., Miyazaki, Y., Takezawa, Y., Nogi, M., Abe, K., Ifuku, S., Yano, H. (2007). Excellent
621 Thermal Conductivity of Transparent Cellulose Nanofiber/Epoxy Resin Nanocomposites.
622 *Biomacromolecules, 8*(9), 2976-2978. doi:10.1021/bm7004998

623 Shiota, A., Ober, C. K. (1997). Rigid rod and liquid crystalline thermosets. *Prog. Polym. Sci., 22*(5),
624 975-1000. doi:10.1016/s0079-6700(97)00014-2

625 Shopsowitz, K. E., Hamad, W. Y., MacLachlan, M. J. (2012). Flexible and Iridescent Chiral Nematic
626 Mesoporous Organosilica Films. *J. Am. Chem. Soc., 134*(2), 867-870. doi:10.1021/ja210355v

627 Shopsowitz, K. E., Qi, H., Hamad, W. Y., MacLachlan, M. J. (2010). Free-standing mesoporous silica
628 films with tunable chiral nematic structures. *Nature (London, U. K.), 468*(7322), 422-425.
629 doi:10.1038/nature09540

630 Sturcova, A., Davies, G. R., Eichhorn, S. J. (2005). Elastic Modulus and Stress-Transfer Properties of
631 Tunicate Cellulose Whiskers. *Biomacromolecules, 6*(2), 1055-1061. doi:10.1021/bm049291k

Szczesniak, L., Rachocki, A., Tritt-Goc, J. (2008). Glass transition temperature and thermal decomposition of cellulose powder. *Cellulose (Dordrecht, Neth.), 15*(3), 445-451. doi:10.1007/s10570-007-9192-2

Talapin, D. V., Shevchenko, E. V., Murray, C. B., Kornowski, A., Foerster, S., Weller, H. (2004). CdSe and CdSe/CdS Nanorod Solids. *J. Am. Chem. Soc., 126*(40), 12984-12988. doi:10.1021/ja046727v

Tan, C., Fung, B. M. (2001). Birefringence and dichroism of oriented epoxy thermoset films. *J. Polym. Sci., Part B Polym. Phys., 39*(9), 915-919. doi:10.1002/polb.1066

Tang, L., Weder, C. (2010). Cellulose Whisker/Epoxy Resin Nanocomposites. *ACS Appl. Mater. Interfaces, 2*(4), 1073-1080. doi:10.1021/am900830h

Tatsumi, M., Teramoto, Y., Nishio, Y. (2012). Polymer Composites Reinforced by Locking-In a Liquid-Crystalline Assembly of Cellulose Nanocrystallites. *Biomacromolecules, 13*(5), 1584-1591. doi:10.1021/bm300310f

Uetani, K., Yano, H. (2012). Semiquantitative Structural Analysis of Highly Anisotropic Cellulose Nanocolloids. *Acs Macro Letters, 1*(6), 651-655. doi:10.1021/mz300109v

Viet, D., Beck-Candanedo, S., Gray, D. G. (2007). Dispersion of cellulose nanocrystals in polar organic solvents. *Cellulose (Dordrecht, Neth.), 14*(2), 109-113. doi:10.1007/s10570-006-9093-9

Yoshiharu, N., Shigenori, K., Masahisa, W., Takeshi, O. (1997). Cellulose microcrystal film of high uniaxial orientation. *Macromolecules, 30*(20), 6395-6397. doi:10.1021/ma970503y

Zhou, J., Liu, S., Qi, J., Zhang, L. (2006). Structure and properties of composite films prepared from cellulose and nanocrystalline titanium dioxide particles. *J. Appl. Polym. Sci., 101*(6), 3600-3608. doi:10.1002/app.22650

Zou, X., Tan, X., Berry, R. (2010). Flexible, iridescent nanocrystalline cellulose film, and method for preparation. WO 2010124378.

Figure 1
Click here to download Figure: Figure 1.doc

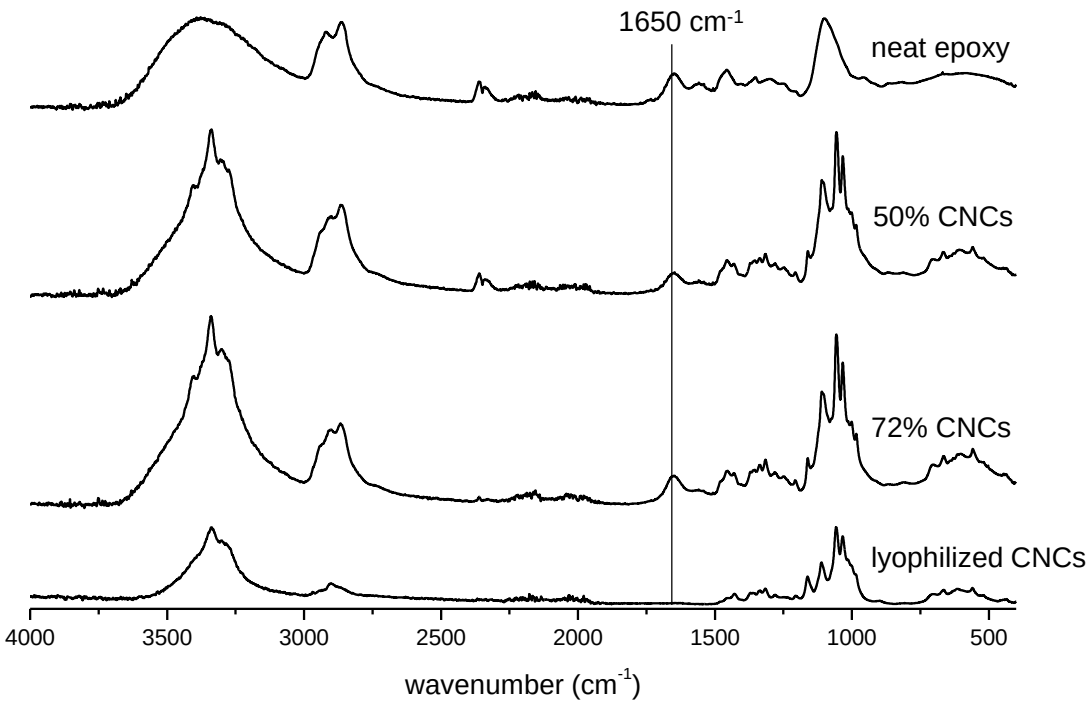

Fig. 1. ATR-FTIR spectra of lyophilized CNCs (bottom), LCT films containing 50 % and 72 % CNCs (middle), and neat epoxy film (top). Note: Line drawn to guide the eye.

Figure 2
Click here to download Figure: Figure 2.doc

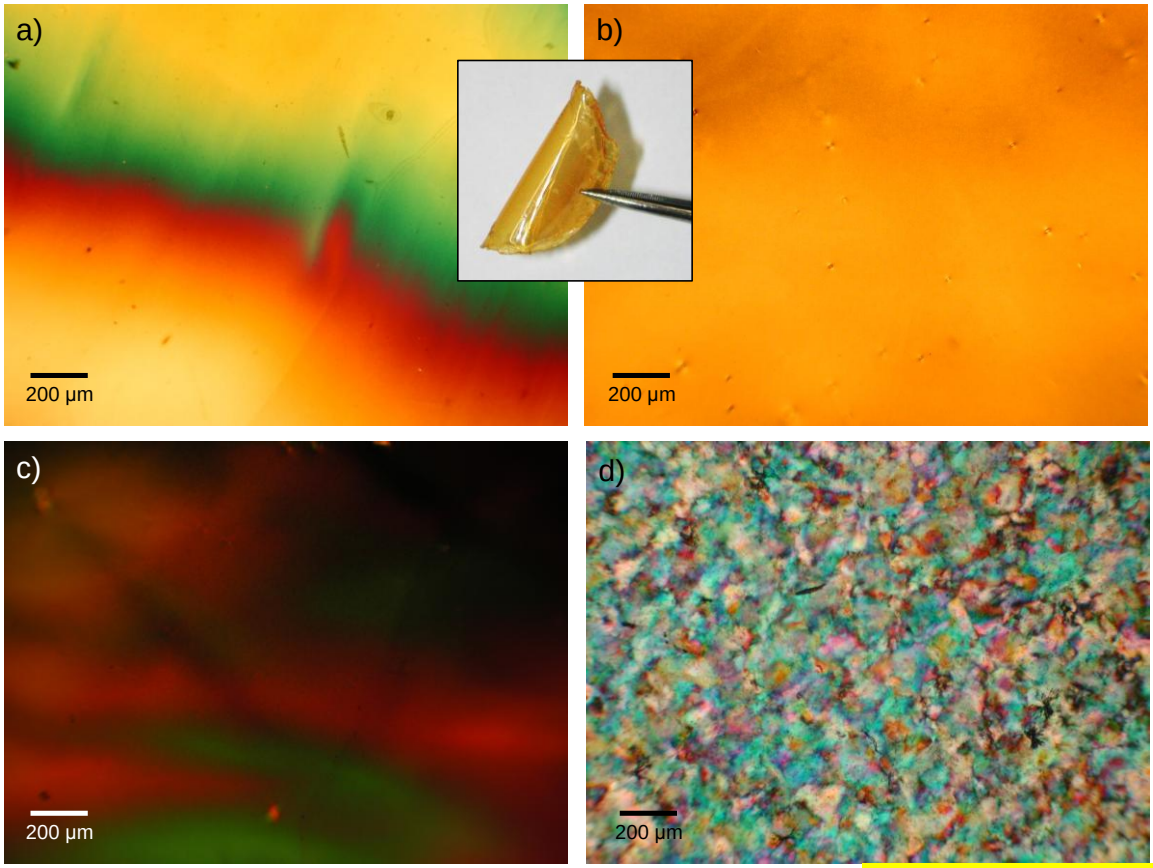

Fig. 2. Typical optical appearance of LCT films (72 % wt. CNCs) at (a) the film edge, (b) ~1 cm from the film edge, (c) the film center under crossed-polarizers, and (d) a pure cellulose nanocrystal film under crossed-polarizers, and (inset) flexed LCT films to the naked eye.

Figure 3
Click here to download Figure: Figure 3.doc

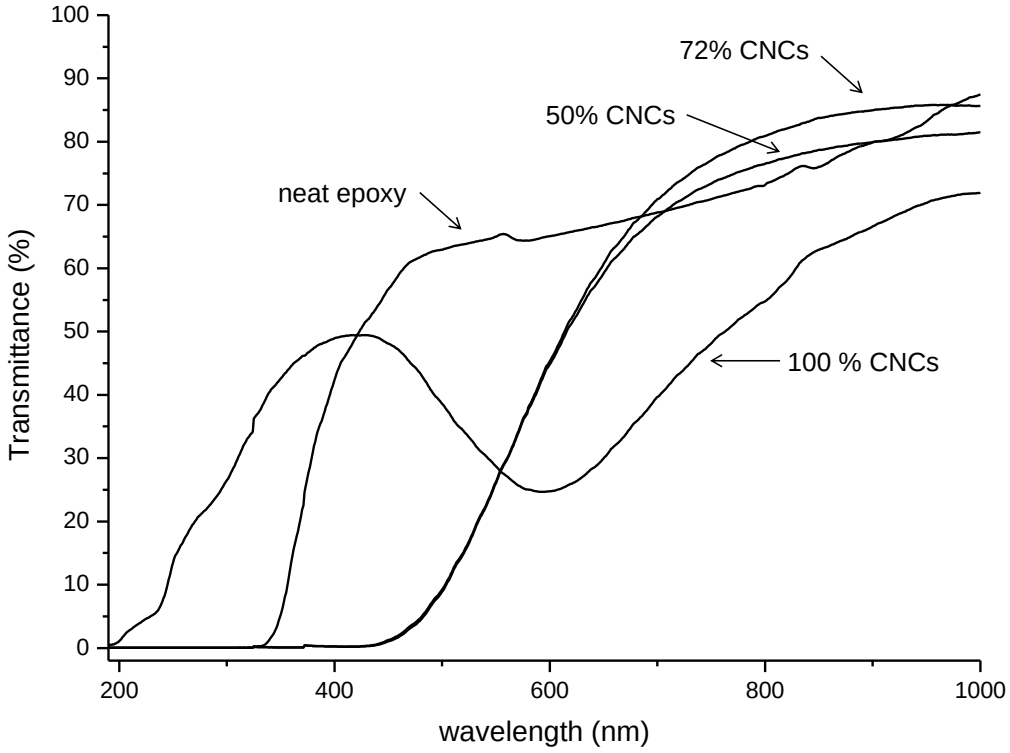

Fig. 3. UV-Vis spectra of a pure CNC film, LCT films containing 50 % and 72 % wt. CNCs, and a neat epoxy film.

Figure 4
Click here to download Figure: Figure 4.doc

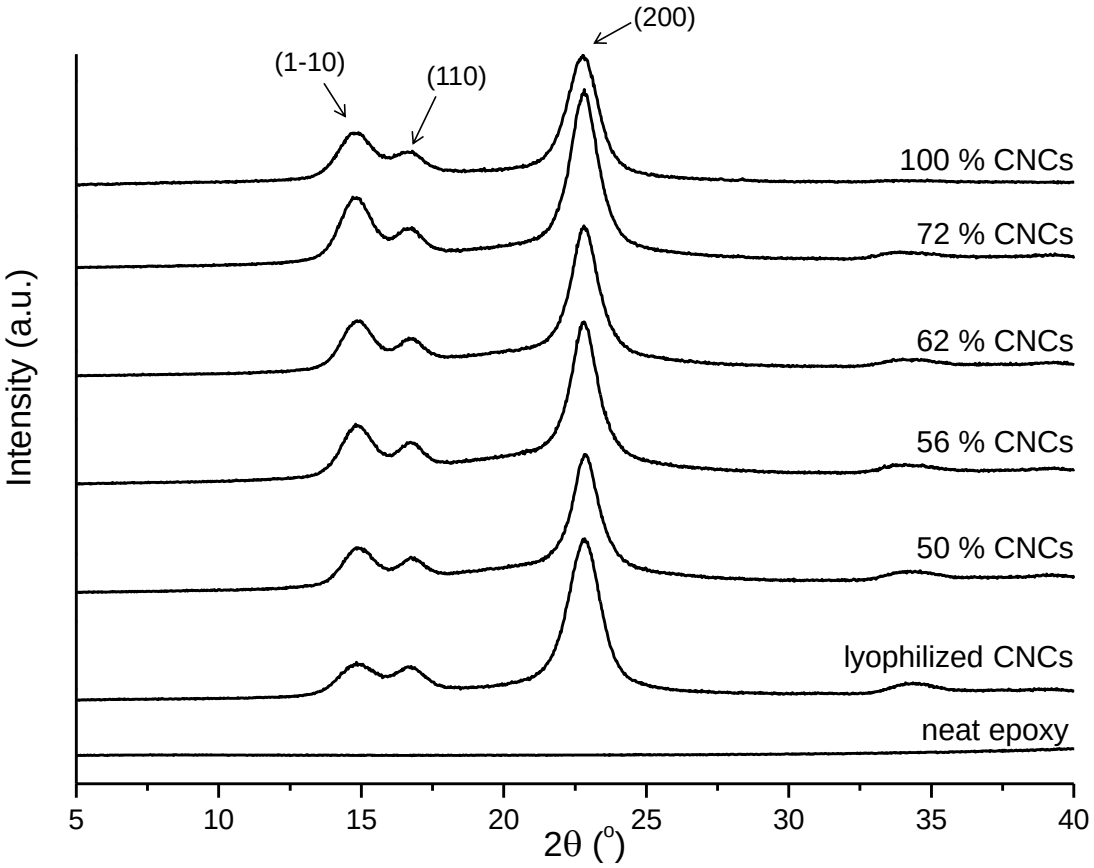

Fig. 4. XRD spectra of a neat epoxy film (bottom), lyophilized CNCs, LCT films containing 50-72 % wt. CNCs and a pure CNC film (top).

Figure 5
Click here to download Figure: Figure 5.doc

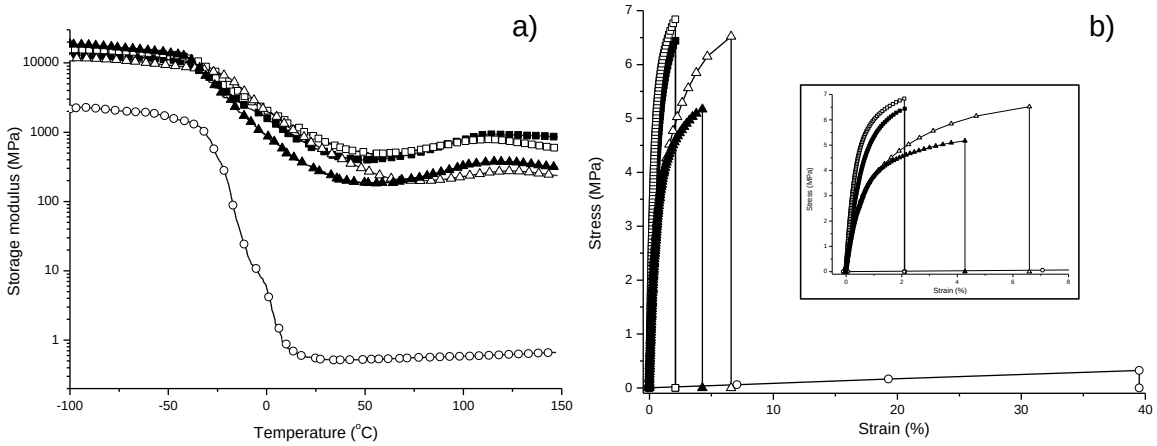

Fig. 5. (a) Evolution of storage modulus (MPa) versus temperature (ºC) and (b) typical stress versus strain curves for LCT films containing 50 % wt. CNCs (-▲-), 56 % wt. CNCs (-Δ-), 62 % wt. CNCs (-□-), 72 % wt. CNCs (-■-) and neat epoxy films (-○-). Notes: Logarithmic scale of the y-axis in (a). Inset plot in (b) contains the same curves from 0 to 8 % strain.

Figure 6
Click here to download Figure: Figure 6.doc

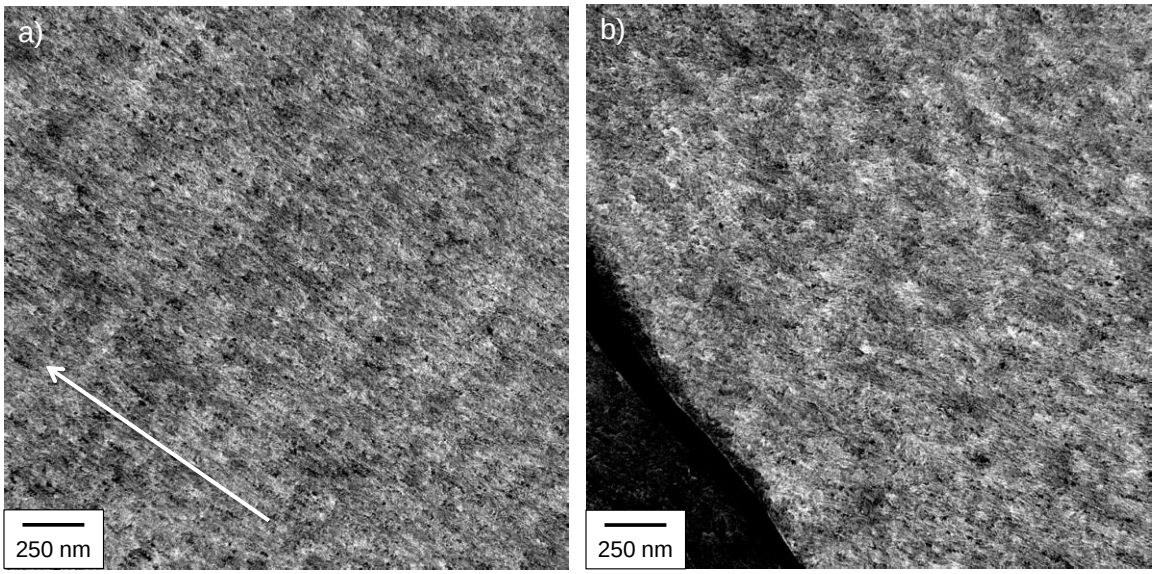

Fig. 6. Typical transmission electron micrographs of LCT films (72 % wt. CNCs) at the (a) edge and (b) center of the film. Notes: Arrow drawn to guide the eye. Dark area in (b) is from the TEM grid.

table 1
Click here to download table: Table 1.doc

Table 1. Average crystallite width (D_{hkl}), crystallinity index (CrI) and intensity ratio ($I_{200}/I_{1\text{-}10}$) of samples derived from XRD spectra.

Sample	*Crystallite width (nm)*[a]	*Crystallinity index (%)*	*Intensity ratio ($I_{200}/I_{1\text{-}10}$)*
Lyophilized CNCs	6.6	90.7	4.0
100% CNCs film	6.4	85.6	2.3
72% epoxy CNCs	7.0	89.3	2.5
62% epoxy CNCs	6.6	86.0	2.6
56% epoxy CNCs	6.5	84.5	2.7
50% epoxy CNCs	6.2	85.1	3.0
neat epoxy	-	-	-

[a]calculated by Scherrer's formula.

Table 2. Summary of thermal transitions of CNCs, LCT films and neat epoxy film from DSC thermograms.

Sample	*Glass transition (T_g) (°C)*	*ΔC_p ($J\,g^{-1}\,°C^{-1}$)*	*% CNCs*	*% epoxy*
Lyophilized CNCs	211	0.395	100	-
72% CNCs	-	-	-	-
62% CNCs	-23.6	0.320	55	45
56% CNCs	-22.3	0.391	45	55
50% CNCs	-22.8	0.404	43	57
neat epoxy	-21.9	0.706	-	100